LAWRENCE
LIVERMORE
NATIONAL
LABORATORY

LLNL-CONF-700381

A Characterization Technique for Nanosecond Gated CMOS X-Ray Cameras

M. Dayton, A. Carpenter, H. Chen, N. Palmer, P. Datte, P. Bell, M. Sanchez, L. Claus, G. Robertson, J. Porter

August 15, 2016

SPIE 2016
San Diego, CA, United States
August 28, 2016 through September 1, 2016

Disclaimer

A Characterization Technique for Nanosecond Gated CMOS X-ray Cameras

M. Dayton[a], A. Carpenter[a], H. Chen[a], N. Palmer[a], P. Datte[a], P. Bell[a], M. Sanchez[b], L. Claus[b], G. Robertson[b], and J. Porter[b]

[a]Lawrence Livermore National Laboratory, Livermore, California
[b]Sandia National Laboratory, Albuquerque, New Mexico

ABSTRACT

We present a characterization technique for nanosecond gated CMOS cameras designed and built by Sandia National Laboratory under their Ultra-Fast X-ray Imager program. The cameras have been used to record images during HED physics experiments at Sandia's Z Facility and at LLNL's National Ignition Facility. The behavior of the camera's fast shutters was not expected to be ideal since they propagate over a large pixel array of 25 mm x 12 mm, which could result in shutter shutter timing skew, variations in the FWHM, and variations in the shutter's peak response. Consequently, a detailed characterization of the camera at the pixel level was critical for interpreting the images. Assuming the pixel's photo-response was linear, the shutter profiles for each pixel were simplified to a pair of sigmoid functions using standard non-linear fitting methods to make the subsequent analysis less computationally intensive. A pixel-level characterization of a "Furi" camera showed frame-to-frame gain variations that could be normalized with a gain mask and significant timing skew at the sensor's center column that could not be corrected. The profiles were also convolved with data generated from computational models to forward fit images collected with the camera.

Keywords: nanosecond gated CMOS-camera, Ultra-Fast X-ray Imager, shutter profiles, flat-fielding

1. INTRODUCTION

Sandia has made novel multi-frame CMOS image sensors under their Ultra-fast x-ray Imager (UXI) program for use in High Energy Density (HED) physics experiments.[1,2] At the National Ignition Facility (NIF), the sensors capture hohlraum dynamics for inertial confinement experiments.[3,4] The images are taken at a high frame rate so they can reveal how fast moving objects change in time, similar to a slow motion video. Poor image quality leads to uncertainties in frame-to-frame measurements that can undermine the experimental results if left unaccounted for or uncorrected, which is why the sensor's limitations must be understood and corrected if possible.

To improve the image's Signal to Noise Ratio (SNR), standard flat fielding techniques are often used to correct for fixed pattern noise, which includes dark signal offsets and photo response nonuniformities of the pixels.[5] For typical applications a standard flat-field correction would be acceptable since the signals of interest change slowly in time compared to shutter speeds and timing skews. However, at NIF the signals change quickly compared with shutter speeds and timing skews. Moreover, standard flat-fielding techniques cannot correct for temporal skews or fluctuations in the shutter response, another method would be needed.

Since the shutter timing skews are not correctable at NIF, they are arguably the most important sensor characteristic. The effects are sometimes referred to as a rolling shutter effect and they can manifest themselves as wobles, bending geometry, and intensity variations. The effects are particularly pronounced when the input signal changes quickly and the timing skews are on the same order as the shutter's Full Width Half Maximum (FWHM). Equation 1 illustrates the dependencies of the image's SNR and assumes that the skews behave

This work was performed under the auspices of the U.S. Department of Energy by Lawrence Livermore National Security, LLC, under Contract No. DE-AC52- 07NA27344.

LLNL-ABS-682120
Matthew Dayton: E-mail: Dayton5@llnl.gov, Telephone: 1-925-424-2153

like a uniformly distributed random variable with a zero mean. In the Equation, variable t_{skew} represents the magnitude of the skew, f is the oscillation frequency of input signal, and FWHM is the shutter's Full Width Half Maximum. Function $g(\cdot)$ summarizes a complicated relationship between the SNR, the frequency content of the input signal, and the FWHM, which does not help show the effects of timing skew on the SNR. Equation 1 does not strictly apply however since the majority of the observed spatial skews are not random in the UXI sensors. Nonetheless, it is helpful to see how the frequency content of the optical signal and the timing skews together can degrade an image's quality. Spatial shutter timing skews are typically caused by variations in the sensors' internal power supply, temperature, and signal cross coupling.

The shutter's shape also affects the camera's signal to noise ratio. Consider a single pixel. If the illuminating light source flickered, then the pixel would perceive a lower intensity than a light source that did not flicker because of the combined integration effect of the photodiode, sense capacitor, and electronic shutter. It would be impossible to distinguish the difference between a constant, but less intense, illumination source and one that was flickering. The effect becomes significant for flicker frequencies on the order of $(2 \times FWHM)^{-1}$. Furthermore, if the flickering was caused by a fast moving object, then it would appear as an image blur across a pixel array. When the shutter does not look like an ideal rectangular function, the effect becomes even more complex where oscillations in the profile's shape can modulate the input signal. In this regard the shutter's profile shape can influence the images signal-to-noise ratio and should be verified.

$$\mathrm{SNR}_{\mathrm{skew}} = \frac{\sqrt{3}}{2\pi f t_{\mathrm{skew}}} g(f, \mathrm{FWHM}) \tag{1}$$

Although it is not possible to correct the images for shutter skews, areas of the sensor with the most timing skew can be avoided. It is also possible to forward fit simulation results to include the sensor effects and compare them with images collected during an experiment.[4] In this paper, we compared the effects of a UXI camera with an ideal camera to assess the impact of the effects. Additionally, as we found in the results, side-to-side timing skews can be leveraged to effectively create more frames.

This paper presents a methodology for acquiring critical pixel level timing information and responsivity that has been used to interpret images taken at NIF. As a usage example of the method and the results that it can produce, the characterization data for a UXI camera called "Furi" is presented. Also in this paper we refer to the frame's electronic pixel shutter simply as the shutter. In other contexts it may be also referred to as a "gate".

2. UXI BACKGROUND

"Furi" is a two frame, common anode device. It is said to be "hybridized" because a custom Readout Integrated Circuit (ROIC) is bonded to an array of Si photodiodes. The photodiodes have a 25 μm pitch and are sensitive to 1-10keV x-rays depending on the starting material. Some versions of the sensors are sensitive to visible light since the face of the photodiode array is not completely metalized. Instead the face of the photodiodes have a metal grid that resembles a waffle pattern and leaves the sensor with fill factor of 77% for visible light. This is useful since visible light is more convenient to work with than x-rays especially with short pulsed sources. A green 532 nm short pulsed laser has an absorption depth equivalent to a 1keV x-ray and would produce characterization results at the lower operating range of the photodiode. Since the Furis photodiode impulse response width is approximately 150 ps at the nominal 50 Volt operating bias, differed charge in the photodiode is not an issue considering the designed shutter width is at least one nanosecond.

The UXI shutter distribution scheme influences timing skews and profile shapes. To shorten the propagation length of each row, the pixel array is bisected vertically into two halves. Each side of the distribution path is then mirrored as seen in Figure 1. The shutters for both sides leave the high speed timing (HST) generator and headed towards their respective 10-stage binary replication tree. The replication tree distributes the shutter to 1024 rows. A row buffer then drives the shutter across its row another 5.6 mm. Before the shutter arrives at the pixel array, it will have propagated through more than 500 gates over a distances of 22 mm. In this type of structure balancing the propagation delays and minimizing timing skew is the major concern.

The UXI designs allows users to select various timing modes. The timing modes are described by the amount of time "on" and then by the amount of time "off" before the next frame. For example, a "2-1" timing mode

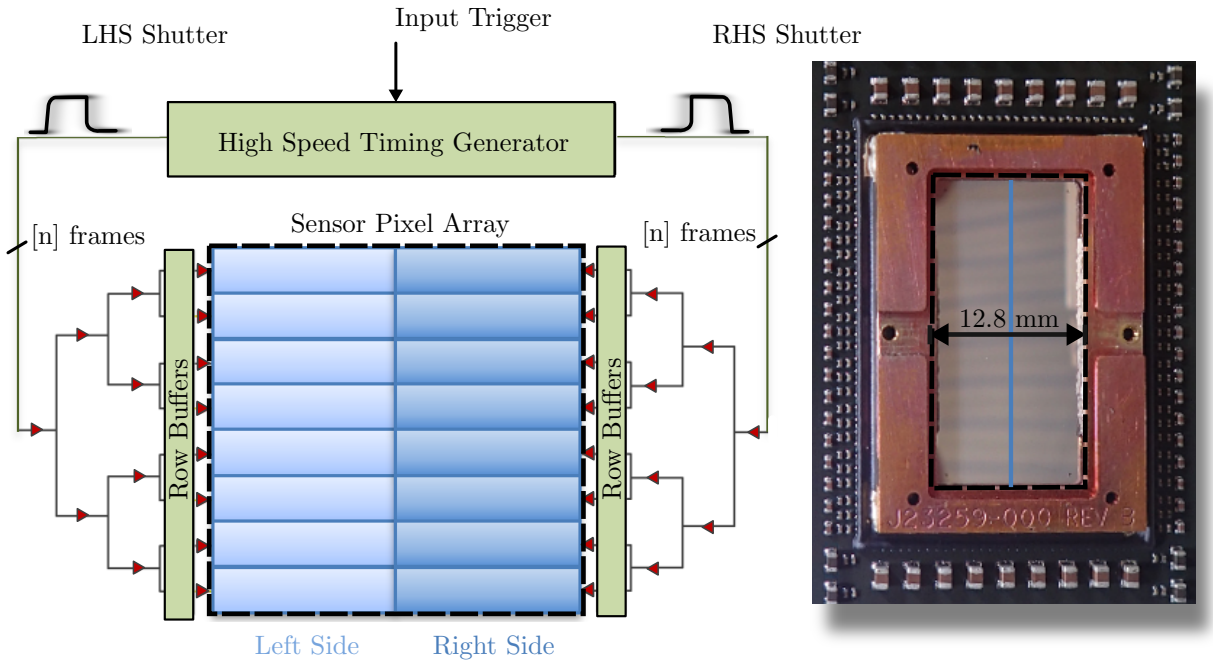

Figure 1: This figure shows the propagation paths for both shutters and a Furi sensor for perspective. Each shutter propagates approximately 22 mm through hundreds of gates to the edge of the sensor"s pixel array. As a consequence, the behavior of the shutters was not expected to be ideal.

means that the shutter's FWHM for each frame's should be two nanoseconds with one nanosecond of dead-time between them. In the UXI family each sensor type has a fixed number of timing modes described in reference.[1] In the camera the shutter widths are programed digitally via an FPGA.

3. METHODOLOGY

The goal of the method was to provide skew, offset, and gain measurements for experimentalists to use for image correction and interpretation. Pixel-level shutter profiles provide all three measurements with a single setup. Furthermore, the profiles were intended to help designers diagnose performance issues and illustrate the underlying architecture of the device with two-dimensional parameter maps.

To obtain the profiles we walked a laser pulse in time through the sensor's shutter seen in figure 2. Each laser shot produced one image per frame and then a region of interest (ROI) was subsequently drawn on them. The median value for each of the ROIs was plotted to represent the frame's shutter value at that point in time. As the laser shots were stepped forward, a shutter profile begins to take shape. The half-maximum of the rising edge defined the start of each shutter profile. Random skews were averaged out since many laser shots form the rising edge of the shutter profile. For the pixel-wise shutter profiles, the region of interest was naturally defined as a single pixel, however, we also used quadrants to summarize the sensor's behavior.

For good resolution of the shutter profile, the profile needed to be oversampled and the laser's pulse width needed to be much shorter than the profile's width. We used a two picosecond laser pulse in the Furi tests, which meant that we could reconstruct detailed shutter profiles for good timing skew measurements. Nonetheless, the finest granularity of the profile was ultimately limited by the photodiode's impulse response width and not the the laser pulse width. The timing measurements were taken with a 12 GHz bandwidth oscilloscope and the cable delays were accounted for to reference all skew measurements to the camera's fine trigger.

Manual camera readout times and scope captures led to unacceptably long acquisition times. In an attempt to increase the throughput and reduce human errors, we automated the tedious process of collecting images and data. After automation, it took three minutes to download a single shot's worth of images and data for the Furi

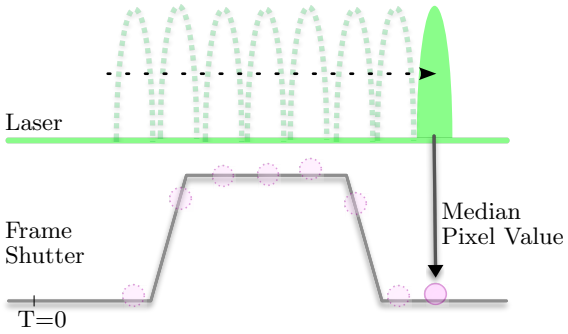

Figure 2: In reference to the frame's shutter, the laser pulse was stepped forward in time. The resulting set of images were captured and the median for each frame's ROI was plotted to form the shutter's profile.

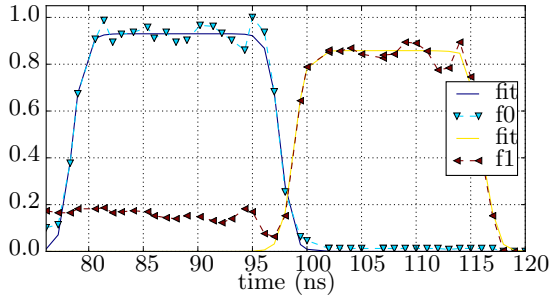

Figure 3: The shutter profiles for 19-1 timing modes are plotted for two Furi frames. The fit function captured the timing and amplitude information for both frames. "f0" refers to frame-0 and "f1" refers to frame-1

tests. Hence, the characterization of a single timing mode took an average of 4 hours and a full characterization of a Furi would take 741 hours since there was 190 possible timing modes. A complete characterization of the newer UXI cameras would take even longer since they had more than four times the possible timing modes. For practical reasons, we calibrated a subset of timing modes that are likely to be used in NIF experiments instead.

Once the images were collected and processed along with the timing information. Each pixel was summarized with four parameters and a fit function. The noiseless fit function did not oscillate, which made the profiles shapes more straight forward to define. For instance the fit function's peak photo-response was no longer ambiguous since there was only one profile peak instead of several. Furthermore, the start of the profile was well defined at the half-maximum of the rising edge. The fit parameters, timing measurements, and amplitude measurements were stored in two-dimensional arrays for easier handling, which was especially true when considering alternative ROIs and performing statistical analysis. Each timing mode test produced nearly a thousand files. To process them for analysis, we developed a bioinformatics-inspired computation pipeline written in Python using Ruffus.[6]

3.1 fit function selection

A parsimonious fit function was used to measure the profile's peak responsivity and its Full Width Half Maximum. The approach of defining a profile with a minimum set of parameters kept the computational effort low. As a result the simple model did not capture some features, such as overshoots, oscillations, and offsets before and after the profile. Figure 3 illustrates this. Additionally, the rise and fall times of the profiles were not always symmetrical as the Equation suggests, however, it would take a trivial extension of the model to capture these parameters if they were desired.

$$fit(t,\beta) = \frac{A}{1-exp(-\frac{t-T_1}{\tau})} - \frac{A}{1-exp(-\frac{t-T_2}{\tau})} \quad , \quad \beta = (A,\tau,T_1,T_2) \tag{2}$$

3.2 roi selection

A large set of pixel profiles was not always desirable. For example, forward fitting simulation data pixel-by-pixel may not be practical for every experiment; therefore, we considered larger ROIs that summarized the shutter profile's behavior.[4] To do this we compared the pixel level timing skews with candidate ROIs and found that the majority of the Furi timing skews could be lumped into quadrants over the sensors active region, which is why some of the analysis uses quadrants. Typical intra-quadrant timing skew was less than 500 ps in Furi. Other applications on the other hand may be more sensitive to timing skews and require eight or more quantiles to summarize the behavior of the shutter timing skews.

4. SETUP

Laser beam uniformity is critical for flat fielding, but beam uniformity is not critical for making shutter profile timing measurements, nor is it critical for comparing the photoresponse from frame to frame. Nonetheless, the beam was diffused with beamline optics to reduce the fixed pattern noise induced by the laser beam. For the Furi tests, the laser beam fluence across the pixel array varied less than 10% from side to side and less than 36% from top to bottom. Beam uniformity was verified using a scientific grade CCD camera and shot-to-shot radiant energy variations were checked with an energy monitor. The trigger system jitter was 25 ps RMS and the cable delays were measured using Time Domain Reflectometry (TDR).

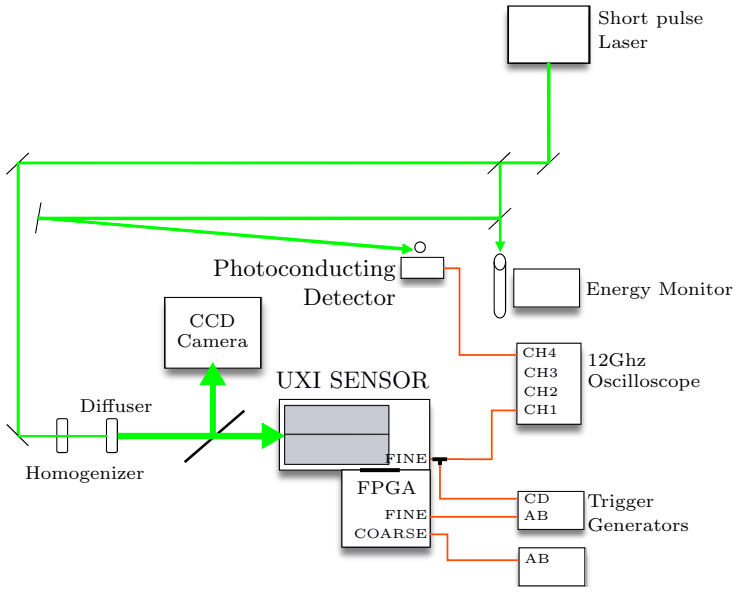

Figure 4: This figure displays the generalized setup for capturing the shutter profiles. A computer,which is not shown, controlled and collected data from the devices show.

5. RESULTS

The characterization results for a Furi sensor provided a usage example of the method. Only the "2-1" timing mode was shown, however eight commonly used timing modes were characterized. A summary of their results are shown in the Appendices. Similar types of results for the Furi have been unofficially presented before, however, none have spanned the entire active region of the sensor.

5.1 shutter profile

The peak shutter profile for the sensor's quadrants varied from frame to frame. The shapes were relatively similar despite distortions in their tails that occurred during the transition from one frame to the other, seen in figure 5 between 81 ns and 83 ns. Laser beam nonuniformity did not explain the 40% difference in the profile's side-to-side peaks, which should have been less than 4%.

5.2 Column timing skew

The shutter timing skews in the pixel columns were discernible between the left half of the sensor and the right half of the sensor. In the 2-1 timing mode, the side-to-side skew was more than 1.2 ns, which was significant considering the frames prescribed 2 ns FWHM. The column timing skew per pixel on the right side was about 2 ps and on the left side it was about 1 ps, seen in figure 6.

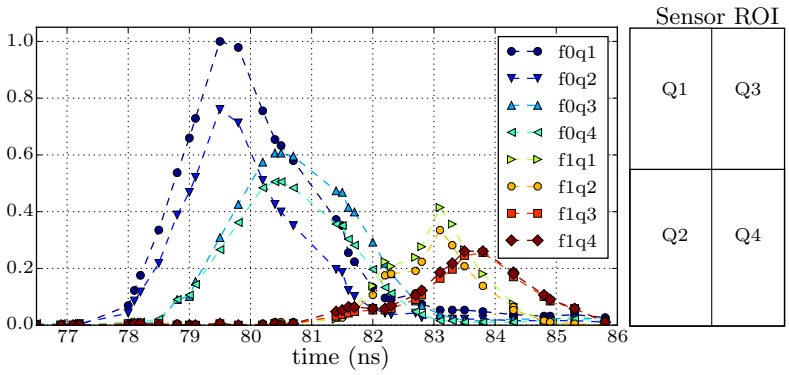

Figure 5: The shutter profiles for the 2-1 timing mode. f0 refers to frame-0 and f1 refers to frame-1. The images were segmented into four quadrants to summarize each area's behavior. The region of interests (ROI) are drawn next to the plot for quick reference.

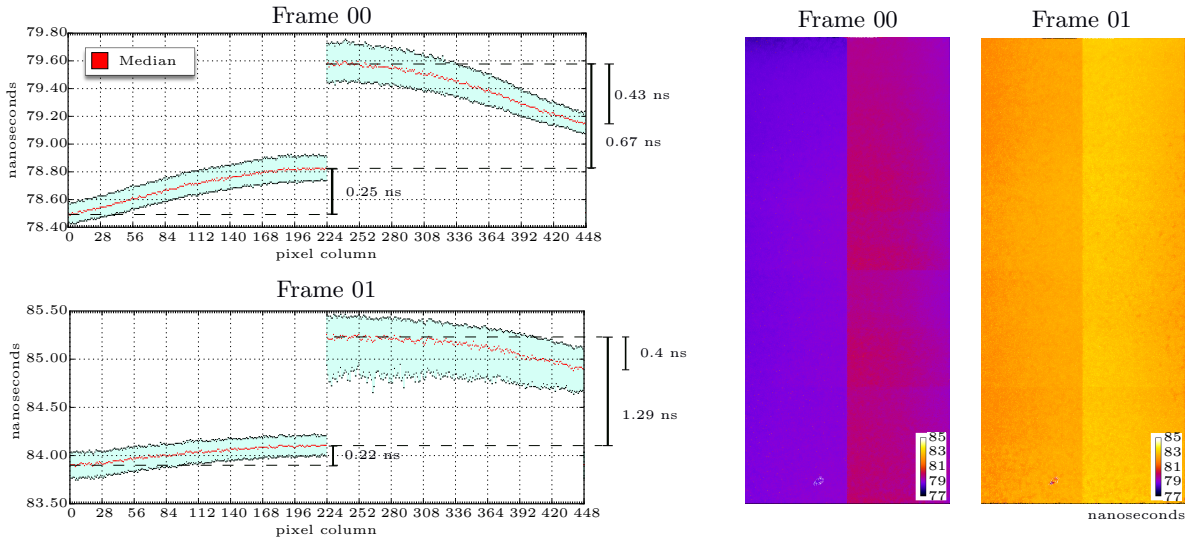

(a) (b)

Figure 6: (a.) The median pixel column skews and their quartiles are shown for each column. (b.) A heatmap representation of the pixel timing skews for each frame

5.3 Row timing skew

Timing skews from top to bottom of the sensor were not as severe as left to right. Nonetheless the variations were 0.35 ns on the right side and 0.51 ns on the left side. Skews in the binary tree stages produced the discrete steps seen in figure. 7.

5.4 Full Width Half Maximum

FWHM was not constant across each frame. The heatmaps in figure 8 show the gradients and some of the ROIC structure that indicated a correlation between the pixels location and the shutter's FWHM. Frame-1's histogram appeared to have a normal distribution about a mean, while frame-0's histogram appeared to be bimodal.

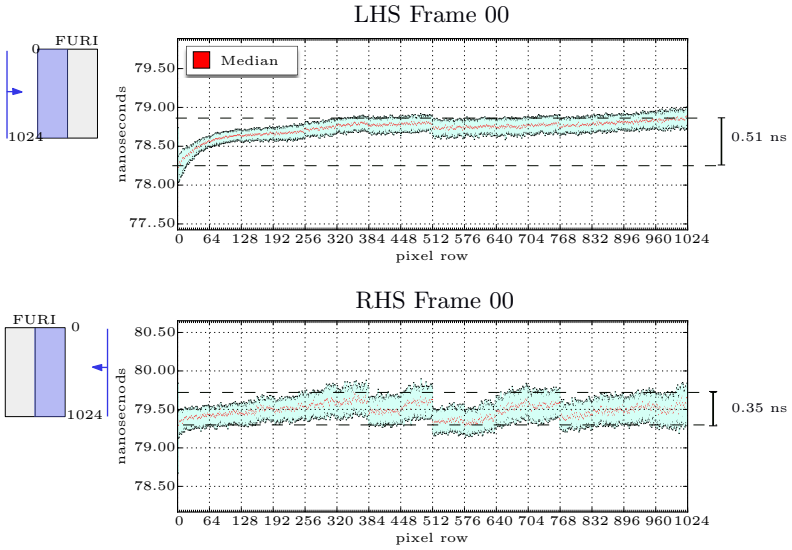

Figure 7: Pixel row timing skews. The median and quartiles are shown for each half of the sensor.

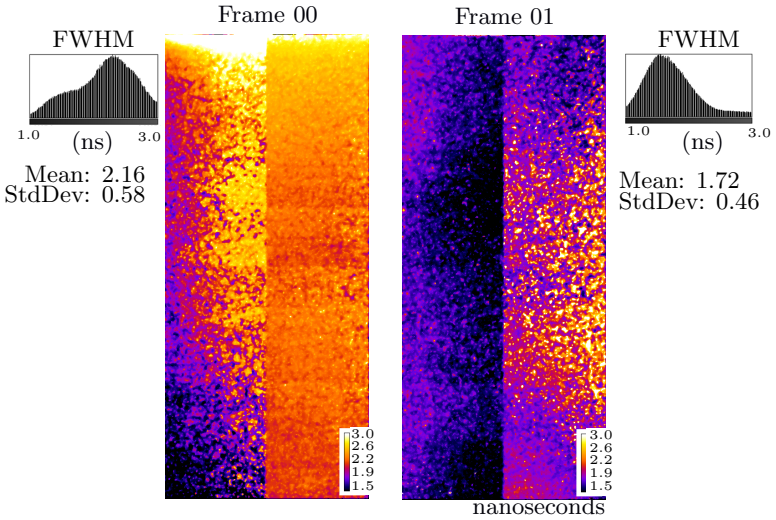

Figure 8: The Heatmap represents the locational distribution of the FWHM of both frames, while the histograms next to each heatmap represents their statistical distribution. Ideally, the values seen in heatmaps would be a uniformly distributed 2 ns, since the 2-1 timing mode was used

5.5 Shutter Profile Impact on Images

To assess the impact of the timing skews and gain variations on NIF images, two simulations were done. The first simulation assumed an ideal rectangular shutter profile and the second assumed frame-0's shutter profiles seen in figure 5. The main features in the images were preserved despite the distortions caused by the non-ideal profile shapes. The results in figure 9 show the effects of gain variations in the image between Q1 and Q2. When comparing the right-half and the left-half of the Furi image, it was harder to differentiate the effects of the gain variations from the timing skews given that the input x-ray intensity signal was changing in time.

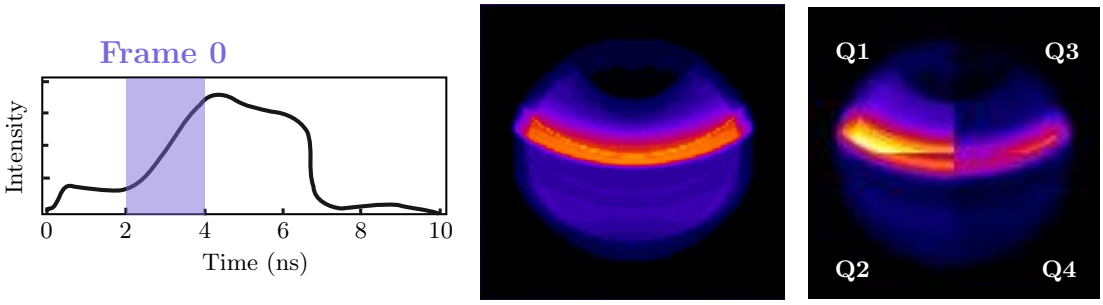

(a) input xray intensity (b) ideal image (c) simulated Furi image

Figure 9: This figure demonstrates how the quadrant shutter profile skews and gain differences can affect an image

6. DISCUSSION

The Furi sensor's side-to-side timing skew was significant when compared with the prescribed two nanosecond shutter. In most cases the sensor behaved more like a four frame device, where the original frame could have been split into two frames alongside each other. Experimentalists should avoid projecting images onto the center of the Furi sensor, unlike what is seen in figure 9, or perhaps they could take advantage of the behavior and project a set images on each side of the sensor for more temporal information.

The sensor also exhibited significant row-wise timing skews that appeared approximately every $2^6 = 64$ rows seen in figure 7. The discrete steps suggested that the majority of the skews accumulated before stage six in the 10-stage binary replication tree. Designers can now use this information to improve the next generation of UXI cameras.

Also, we found that the peak shutter response varied from frame-to-frame, which could explain some of the image intensity differences experimentalists observed between frames at NIF. The cause may be related to large current transients that produced voltage drops on the power rails during the propagation of the shutters and the high-peak currents produced from the transient photocarrier signal. Nonetheless, it would be desirable to normalize this Frame-to-Frame effect, and hence, a gain correction mask was derived with the ratio of the two frame's peak profile values for each pixel seen in Equation 3. The resulting mask is displayed in figure 10 and assumes that the FWHM of both frames were approximately the same shape. The mask does not correct for intensity variations between frames caused by intra-frame timing skews and FWHM variations.

$$\text{mask} = \max_{t \in profile}(\text{Frame0}(t)) / \max_{t \in profile}(\text{Frame1}(t)) \tag{3}$$

The test results gave some indication of inter-frame coupling for the 19-1 timing mode that can be seen in figure 3. The source was likely not deferred charge in the photodiode because the photodiode's response was shorter than the shutter's FWHM and the frame's charge transfer gate should have isolated the pixel's sense capacitor.

7. CONCLUSIONS AND FUTURE WORKS

A pixel-by-pixel understanding of the sensor did not only help experimentalist interpret their images, but it also benefited Sandia's designers. The pixel level timing skews and shutter profile shapes allowed designers to diagnose and correct possible biasing and layout issues. Nonuniformities in the shutter profiles also highlighted the need to characterize the UXI sensor prior to using it for time resolved experiments.

To increase the setup's throughput, a new set of camera boards were designed and built to readout four images within five seconds. Scope readouts were also minimized to a few seconds. With the new electronics and oscilloscope setup, we could acquire shutter profiles in a matter of minutes instead of hours, which makes optimizing the sensors operating voltages more practical. In the near future we plan to characterize Sandia's

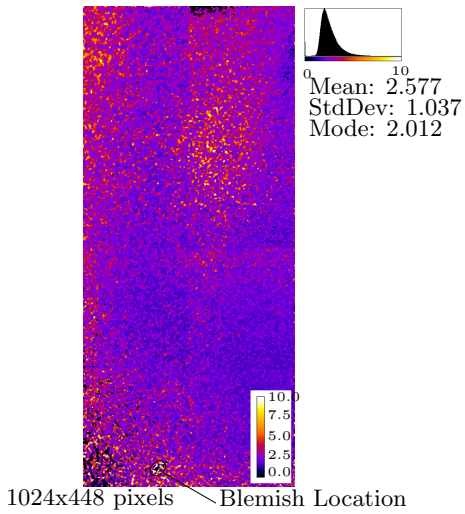

Figure 10: A heatmap representation of the frame-to-frame normalization mask for timing mode 2-1. The histogram next to the mask shows the statistical distribution of the normalization values. On average, frame-0's shutter profile was 2.57 times frame-1's. If the profile amplitudes were ideal, the average would be 1.00 and the heatmap would appear to be uniform.

next generation of sensor called Icarus using the methods described in this paper. The consistent methodology will make it easier to benchmark the sensor's performance with other UXI sensors.

APPENDIX A. PHOTON TRANSFER CURVE

Photodiode linearity must also be verified, however it was not the focus of this paper. there are many techniques available for doing this. We inserted calibrated ND filters in the beam-line to illuminate the sensor over the theoretical illumination range of the photodiode. As seen in figure 11, the full-well capacity was never reached. Since the UXI sensor and camera would upset when the entire sensor was illuminated above 20%, a smaller ROI of 21,000 pixels was illuminated instead. The ADC gain could not be obtained graphically because the camera was not shot noise limited in the optical regime. Since the camera does not use double correlated sampling the reset noise can be signification, however, it is still not clear why the readout noise was so high.

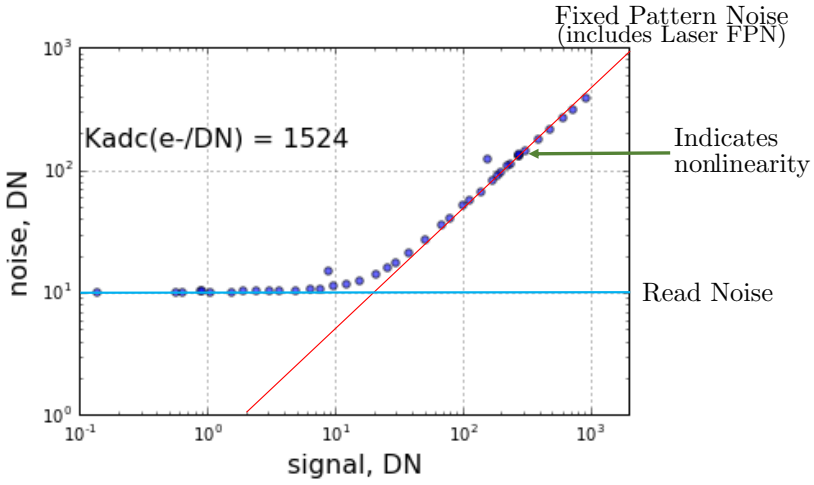

Figure 11: The classical photon transfer curve. The fixed pattern noise was mostly caused by speckling in the laser beam. Full-well capacity was not achieved during this test.

APPENDIX B. FURI TIMING MODE PERFORMANCE SUMMARIES

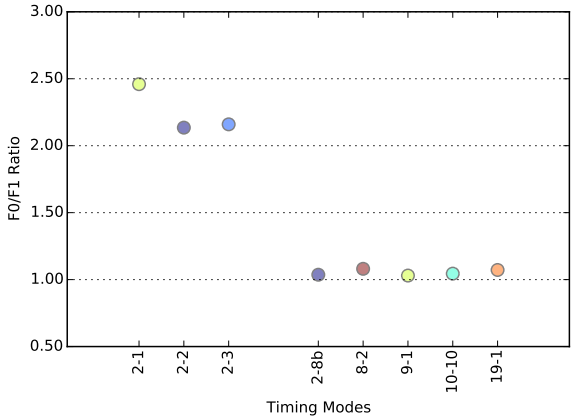

Figure 12: A Comparison of the shutter profile peak of frame-0 divided by shutter profile peak of frame-1 for various Furi timing modes. A ratio of one is ideal.

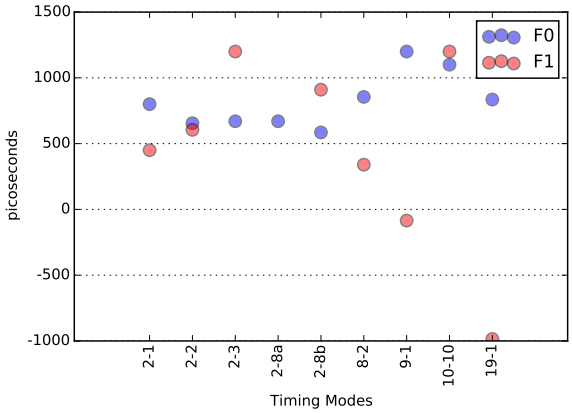

Figure 13: Timing skews from the left-hand side of the Furi sensor compared to the right-hand-side. The ideal skew between the two sides is zero. Therefore, frame1 in the 9-1 timing mode performed the best.

REFERENCES

[1] Claus, L., Fang, L., Kay, R., Kimmel, M., Long, J., Robertson, G., Sanchez, M., Stahoviak, J., Trotter, D., and Porter, J., "An overview of the ultrafast x-ray imager (uxi) program at sandia labs," in [*SPIE Optical Engineering+ Applications*], 95910P–95910P, International Society for Optics and Photonics (2015).

[2] Porter, J. et al., "A hybrid cmos sensor with multi-frame storage for high-speed x-ray imaging," The 20th Topical Conference on High Temperature Plasma Diagnostic (2014).

[3] Palmer, N. E., Chen, H., Nelson, J., Heerey, S., Piston, K., Thao, M., Schneider, M., Bell, P., Bradley, D., Porter, J., et al., "Design and implementation of a gated-laser entrance hole imaging diagnostic (g-leh-1) at nif," in [*SPIE Optical Engineering+ Applications*], 959106–959106, International Society for Optics and Photonics (2015).

[4] Chen, H., Palmer, N. E., Dayton, M., Carpenter, A., et al., "A high-speed two-frame, 1-2ns gated x-ray cmos imager used as a holhraum diagnostic on the national ignition facility," in [*The 21th Topical Conference on High Temperature Plasma Diagnostic*], American Physical Society (2016).

[5] "Photography–electronic still-picture imaging-noise measurements," ISO ISO 15739:2013, International Organization for Standardization (2013).

[6] Leipzig, J., "A review of bioinformatic pipeline frameworks," *Briefings in bioinformatics* , bbw020 (2016).